

A spatospectral localization approach for analyzing and representing vector-valued functions on spherical surfaces

Alain Plattner and Frederik J. Simons

Department of Geosciences, Princeton University, Guyot Hall, Princeton, NJ, USA

ABSTRACT

We review the construction of three different Slepian bases on the sphere, and illustrate their theoretical behavior and practical use for solving ill-posed satellite inverse problems. The first basis is scalar, the second vectorial, and the third suitable for the vector representation of the harmonic potential fields on which we focus our analysis. When data are noisy and incompletely observed over contiguous domains covering parts of the sphere at satellite altitude, expanding the unknown solution in terms of a Slepian basis and seeking truncated expansions to achieve least-squares data fit has advantages over conventional approaches that include the ease with which the solutions can be computed, and a clear statistical understanding of the competing effects of solution bias and variance in modulating the mean squared error, as we illustrate with several new examples.

Keywords: vector spherical harmonics, statistical methods, inverse theory, satellite geodesy, geomagnetism

1. SCALAR AND VECTORIAL SPHERICAL SLEPIAN FUNCTIONS

1.1. Scalar spherical harmonics

With $\hat{\mathbf{r}} = (\theta, \phi)$, colatitude $0 \leq \theta \leq \pi$ and longitude $0 \leq \phi < 2\pi$ on the unit sphere $\Omega = \{\mathbf{x} \in \mathbb{R}^3 \mid \|\mathbf{x}\| = 1\}$, the real *surface* spherical-harmonic functions are, for degree $l > 0$ and order $-m \leq l \leq m$,

$$Y_{lm}(\hat{\mathbf{r}}) = Y_{lm}(\theta, \phi) = \begin{cases} \sqrt{2}X_{l|m|}(\theta) \cos m\phi & \text{if } -l \leq m < 0, \\ X_{l0}(\theta) & \text{if } m = 0, \\ \sqrt{2}X_{lm}(\theta) \sin m\phi & \text{if } 0 < m \leq l, \end{cases} \quad (1)$$

$$X_{lm}(\theta) = (-1)^m \left(\frac{2l+1}{4\pi} \right)^{1/2} \left[\frac{(l-m)!}{(l+m)!} \right]^{1/2} P_{lm}(\cos \theta), \quad (2)$$

$$P_{lm}(\mu) = \frac{1}{2^l l!} (1-\mu^2)^{m/2} \left(\frac{d}{d\mu} \right)^{l+m} (\mu^2 - 1)^l. \quad (3)$$

The spherical harmonics Y_{lm} defined in (1) form an orthonormal basis for square-integrable real-valued functions on the unit sphere Ω . We can describe any such *scalar* function $f(\hat{\mathbf{r}})$ as a unique linear combination

$$f(\hat{\mathbf{r}}) = \sum_{l=0}^{\infty} \sum_{m=-l}^l f_{lm} Y_{lm}(\hat{\mathbf{r}}), \quad \text{where} \quad f_{lm} = \int_{\Omega} f(\hat{\mathbf{r}}) Y_{lm}(\hat{\mathbf{r}}) d\Omega. \quad (4)$$

1.2. Scalar Slepian functions

To maximize the spatial concentration of a *bandlimited* real-valued spherical scalar function

$$G(\hat{\mathbf{r}}) = \sum_{l=0}^L \sum_{m=-l}^l g_{lm} Y_{lm}(\hat{\mathbf{r}}) \quad (5)$$

within a region R , we maximize the energy ratio

$$\lambda = \int_R G^2 d\Omega \Big/ \int_{\Omega} G^2 d\Omega = \text{maximum}. \quad (6)$$

Maximizing eq. (6) leads to a positive spectral-domain eigenvalue equation for the $\mathbf{g} = (g_{00} \cdots g_{lm} \cdots g_{LL})^T$,

$$\sum_{l'=0}^L \sum_{m'=-l'}^{l'} D_{lm,l'm'} g_{l'm'} = \lambda g_{lm}, \quad 0 \leq l \leq L, \quad (7a)$$

$$D_{lm,l'm'} = \int_R Y_{lm} Y_{l'm'} d\Omega. \quad (7b)$$

The solutions g_{lm} to eq. (7) form the Slepian functions $G(\hat{\mathbf{r}})$ via eq. (5). The latter are orthogonal over R and Ω , and have been studied extensively.¹

1.3. Vector spherical harmonics

With coordinates $(\hat{\mathbf{r}}, \hat{\boldsymbol{\theta}}, \hat{\boldsymbol{\phi}})$ and a surface gradient $\nabla_1 = \hat{\boldsymbol{\theta}} \partial_\theta + \hat{\boldsymbol{\phi}} (\sin \theta)^{-1} \partial_\phi$, the *vector* spherical harmonics are

$$\mathbf{P}_{lm}(\hat{\mathbf{r}}) = \hat{\mathbf{r}} Y_{lm}(\hat{\mathbf{r}}), \quad (8)$$

$$\mathbf{B}_{lm}(\hat{\mathbf{r}}) = \frac{\nabla_1 Y_{lm}(\hat{\mathbf{r}})}{\sqrt{l(l+1)}} = \frac{[\hat{\boldsymbol{\theta}} \partial_\theta + \hat{\boldsymbol{\phi}} (\sin \theta)^{-1} \partial_\phi] Y_{lm}(\hat{\mathbf{r}})}{\sqrt{l(l+1)}}, \quad (9)$$

$$\mathbf{C}_{lm}(\hat{\mathbf{r}}) = \frac{-\hat{\mathbf{r}} \times \nabla_1 Y_{lm}(\hat{\mathbf{r}})}{\sqrt{l(l+1)}} = \frac{[\hat{\boldsymbol{\theta}} (\sin \theta)^{-1} \partial_\phi - \hat{\boldsymbol{\phi}} \partial_\theta] Y_{lm}(\hat{\mathbf{r}})}{\sqrt{l(l+1)}}, \quad (10)$$

noting that the purely radial $\mathbf{P}_{00} = (4\pi)^{-1/2} \hat{\mathbf{r}}$, and $\mathbf{B}_{00} = \mathbf{0}$, $\mathbf{C}_{00} = \mathbf{0}$. The expansion of a real-valued square-integrable *vector* field $\mathbf{f}(\hat{\mathbf{r}})$ on the unit sphere Ω can be written as

$$\mathbf{f}(\hat{\mathbf{r}}) = \sum_{l=0}^{\infty} \sum_{m=-l}^l f_{lm}^P \mathbf{P}_{lm}(\hat{\mathbf{r}}) + f_{lm}^B \mathbf{B}_{lm}(\hat{\mathbf{r}}) + f_{lm}^C \mathbf{C}_{lm}(\hat{\mathbf{r}}), \quad \text{where} \quad (11a)$$

$$f_{lm}^P = \int_{\Omega} \mathbf{P}_{lm}(\hat{\mathbf{r}}) \cdot \mathbf{f}(\hat{\mathbf{r}}) d\Omega, \quad f_{lm}^B = \int_{\Omega} \mathbf{B}_{lm}(\hat{\mathbf{r}}) \cdot \mathbf{f}(\hat{\mathbf{r}}) d\Omega, \quad \text{and} \quad f_{lm}^C = \int_{\Omega} \mathbf{C}_{lm}(\hat{\mathbf{r}}) \cdot \mathbf{f}(\hat{\mathbf{r}}) d\Omega, \quad (11b)$$

using the standard vector dot-product notation and keeping in mind that $f_{00}^B = f_{00}^C = 0$ in the above expression.

1.4. Vectorial Slepian functions

Vector Slepian functions maximize the spatial concentration of a *bandlimited* real spherical vector function

$$\mathbf{g}(\hat{\mathbf{r}}) = \sum_{l=0}^L \sum_{m=-l}^l g_{lm}^P \mathbf{P}_{lm}(\hat{\mathbf{r}}) + g_{lm}^B \mathbf{B}_{lm}(\hat{\mathbf{r}}) + g_{lm}^C \mathbf{C}_{lm}(\hat{\mathbf{r}}) \quad (12)$$

within a certain spatial region R , via the energy ratio

$$\nu = \int_R \mathbf{g} \cdot \mathbf{g} d\Omega \Big/ \int_{\Omega} \mathbf{g} \cdot \mathbf{g} d\Omega = \text{maximum}. \quad (13)$$

The maximization of eq. (13) leads to a coupled system of positive-definite eigenvalue equations,

$$\sum_{l'=0}^L \sum_{m'=-l'}^{l'} D_{lm,l'm'} g_{l'm'}^P = \nu g_{lm}^P, \quad 0 \leq l \leq L, \quad (14a)$$

$$\sum_{l'=0}^L \sum_{m'=-l'}^{l'} B_{lm,l'm'} g_{l'm'}^B + C_{lm,l'm'} g_{l'm'}^C = \nu g_{lm}^B, \quad 0 \leq l \leq L, \quad (14b)$$

$$\sum_{l'=0}^L \sum_{m'=-l'}^{l'} C_{lm,l'm'}^T g_{l'm'}^B + B_{lm,l'm'} g_{l'm'}^C = \nu g_{lm}^C, \quad 0 \leq l \leq L. \quad (14c)$$

The matrix elements that complement the equations above are

$$D_{lm,l'm'} = \int_R \mathbf{P}_{lm} \cdot \mathbf{P}_{l'm'} d\Omega = \int_R Y_{lm} Y_{l'm'} d\Omega, \quad (15a)$$

$$B_{lm,l'm'} = \int_R \mathbf{B}_{lm} \cdot \mathbf{B}_{l'm'} d\Omega = \int_{\mathcal{R}} \mathbf{C}_{lm} \cdot \mathbf{C}_{l'm'} d\Omega, \quad (15b)$$

$$C_{lm,l'm'} = \int_R \mathbf{B}_{lm} \cdot \mathbf{C}_{l'm'} d\Omega, \quad (15c)$$

and the transpose of eq. (15c) switches its sign. The radial vectorial concentration problem (14a), (15a) is identical to the corresponding scalar case (7a)–(7b), and can be solved separately from the tangential equations.²

The eigenfield $\mathbf{g}_1(\hat{\mathbf{r}})$ with the largest eigenvalue λ_1 is the element in the space of bandlimited vector fields with most of its spatial energy within region R , the next best-concentrated bandlimited function $\mathbf{g}_2(\hat{\mathbf{r}})$ is orthogonal to $\mathbf{g}_1(\hat{\mathbf{r}})$ over both Ω and R , and so on for generic λ_α . The sum of the eigenvalues defines a “Shannon number”,

$$N^{\text{vec}} = \sum_{\alpha} \lambda_{\alpha} = [3(L+1)^2 - 2] \frac{A}{4\pi}. \quad (16)$$

Since the radial and tangential eigensolutions are decoupled we may subdivide the vectorial spherical Shannon number into a radial and a tangential one, $N^r = (L+1)^2 A / (4\pi)$ and $N^t = [2(L+1)^2 - 2] A / (4\pi)$, respectively.

An example of tangential vectorial Slepian functions for North America is found in Figure 1.

2. GRADIENT-VECTOR FUNCTIONS FOR POTENTIAL FIELDS

2.1. Potential Functions on the Sphere

With $\nabla^2 = \partial_r^2 + 2r^{-1}\partial_r + r^{-2}\nabla_1^2$, Laplace’s equation defines the three-dimensional *harmonic* functions $V(r\hat{\mathbf{r}})$,

$$\nabla^2 V(r\hat{\mathbf{r}}) = 0. \quad (17)$$

The general solutions of eq. (17) are the inner, $r^l Y_{lm}$, and outer, $r^{-l-1} Y_{lm}$, *solid* spherical harmonics which serve to approximate external-source and internal-source scalar potentials, respectively.^{3–5} The evaluation on a sphere Ω_{r_a} of radius $r_a \geq r_e$, of a function $V(r\hat{\mathbf{r}})$ that satisfies eq. (17) outside a ball of radius r_e , and which vanishes at infinity, is an expansion in spherical harmonics (note that the integrations are over the unit sphere Ω),

$$V(r_a\hat{\mathbf{r}}) = \sum_{l=0}^{\infty} \sum_{m=-l}^l u_{lm}^{r_a} Y_{lm}(\hat{\mathbf{r}}), \quad \text{where} \quad u_{lm}^{r_a} = \int_{\Omega} V(r_a\hat{\mathbf{r}}) Y_{lm}(\hat{\mathbf{r}}) d\Omega. \quad (18)$$

We evaluate $V(r\hat{\mathbf{r}})$ at another radius $r \geq r_e$ from the spherical-harmonic coefficients $u_{lm}^{r_a}$ at radius $r_a \geq r_e$, as

$$V(r\hat{\mathbf{r}}) = \sum_{l=0}^{\infty} \sum_{m=-l}^l \left(\frac{r}{r_a}\right)^{-l-1} u_{lm}^{r_a} Y_{lm}(\hat{\mathbf{r}}). \quad (19)$$

Assuming that Earth’s surface is a sphere Ω_{r_e} of fixed radius r_e , and that the satellite altitude is a sphere Ω_{r_s} of radius $r_s \geq r_e$, using eqs (18)–(19) we can express the potential field $V(r_s\hat{\mathbf{r}})$ at the satellite altitude r_s via the spherical-harmonic coefficients $u_{lm}^{r_e}$ on Earth’s surface r_e by

$$V(r_s\hat{\mathbf{r}}) = \sum_{l=0}^{\infty} \sum_{m=-l}^l \left(\frac{r_s}{r_e}\right)^{-l-1} u_{lm}^{r_e} Y_{lm}(\hat{\mathbf{r}}), \quad \text{where} \quad u_{lm}^{r_e} = \int_{\Omega} V(r_e\hat{\mathbf{r}}) Y_{lm}(\hat{\mathbf{r}}) d\Omega. \quad (20)$$

The potential coefficients $u_{lm}^{r_e}$ can be determined from the radial component of its gradient,⁶

$$\nabla V(r_s\hat{\mathbf{r}}) \cdot \hat{\mathbf{r}} = \partial_r V(r_s\hat{\mathbf{r}}) = \sum_{l=0}^{\infty} \sum_{m=-l}^l -(l+1) r_e^{-1} \left(\frac{r_s}{r_e}\right)^{-l-2} u_{lm}^{r_e} Y_{lm}(\hat{\mathbf{r}}). \quad (21)$$

We define the diagonal upward-transformation matrix \mathbf{A} by its elements

$$A_{lm,l'm'} = -(l+1)r_e^{-1} \left(\frac{r_s}{r_e}\right)^{-l-2} \delta_{ll'} \delta_{mm'}. \quad (22)$$

With perfect knowledge of the radial component of ∇V , the potential V would be uniquely determined. When the data are contaminated by noise, we gain by taking the radial and both tangential components into account.

2.2. Gradient-vector harmonics

A basis of normalized vector spherical harmonics, $\mathbf{E}, \mathbf{F}, \mathbf{C}$, an alternative^{7,8} to the basis $\mathbf{P}, \mathbf{B}, \mathbf{C}$ defined in Section 1.3, is obtained by defining $\mathbf{E}_{00} = \mathbf{P}_{00}$, and, for $l \geq 1$ and $-l \leq m \leq l$, forming the linear combinations

$$\mathbf{E}_{lm} = \sqrt{\frac{l+1}{2l+1}} \mathbf{P}_{lm} - \sqrt{\frac{l}{2l+1}} \mathbf{B}_{lm}, \quad \text{and} \quad \mathbf{F}_{lm} = \sqrt{\frac{l}{2l+1}} \mathbf{P}_{lm} + \sqrt{\frac{l+1}{2l+1}} \mathbf{B}_{lm}. \quad (23)$$

The gradient of the potential at satellite altitude can be written in this basis as

$$\nabla V(r_s \hat{\mathbf{r}}) = \sum_{l=0}^{\infty} \sum_{m=-l}^l -\sqrt{(l+1)(2l+1)} r_e^{-1} \left(\frac{r_s}{r_e}\right)^{-l-2} u_{lm}^{r_e} \mathbf{E}_{lm}(\hat{\mathbf{r}}) = \sum_{l=0}^{\infty} \sum_{m=-l}^l v_{lm}^{r_s} \mathbf{E}_{lm}(\hat{\mathbf{r}}).$$

We refer to the \mathbf{E}_{lm} as *gradient-vector* spherical harmonics. We introduce another diagonal upward-transformation matrix, \mathbf{B} , which has the elements

$$B_{lm,l'm'} = -\sqrt{(l+1)(2l+1)} r_e^{-1} \left(\frac{r_s}{r_e}\right)^{-l-2} \delta_{ll'} \delta_{mm'}. \quad (24)$$

2.3. Gradient-vector Slepian functions

We construct the gradient-vector Slepian functions as the bandlimited gradient-vector harmonic expansion

$$\mathbf{H}(\hat{\mathbf{r}}) = \sum_{l=0}^L \sum_{m=-l}^l h_{lm} \mathbf{E}_{lm}(\hat{\mathbf{r}}), \quad (25)$$

collecting $\mathbf{h} = (h_{00} \cdots h_{lm} \cdots h_{LL})^T$, that solves the spatial maximization problem over the region R ,

$$\sigma = \int_R \mathbf{H} \cdot \mathbf{H} d\Omega \Big/ \int_{\Omega} \mathbf{H} \cdot \mathbf{H} d\Omega = \text{maximum}. \quad (26)$$

An example of gradient-vector Slepian functions for North America is found in Figure 2.

3. POTENTIAL-FIELD ESTIMATION PROBLEMS IN SPHERICAL HARMONICS

We distinguish and treat variations on the following four problems in satellite potential-field estimation.

3.1. P1: Scalar potential data, scalar-harmonic potential coefficients, same altitude

Let there be k values of the *scalar* potential measured at k different points satellite altitude r_s ,

$$\mathbf{V} = \left(V(r_s \hat{\mathbf{r}}_1) \quad \cdots \quad V(r_s \hat{\mathbf{r}}_k) \right)^T, \quad \text{where} \quad V(r_s \hat{\mathbf{r}}_i) = \sum_{l=0}^{\infty} \sum_{m=-l}^l u_{lm}^{r_s} Y_{lm}(\hat{\mathbf{r}}_i). \quad (27)$$

Our objective is to estimate the spherical-harmonic coefficients $u_{lm}^{r_s}$ within a certain bandwidth L . Defining

$$\mathbf{Y} = \begin{pmatrix} Y_{00}(\hat{\mathbf{r}}_1) & \cdots & Y_{00}(\hat{\mathbf{r}}_k) \\ \vdots & & \vdots \\ Y_{LL}(\hat{\mathbf{r}}_1) & \cdots & Y_{LL}(\hat{\mathbf{r}}_k) \end{pmatrix}, \quad (28)$$

and the bandlimited vector of coefficients to be estimated

$$\tilde{\mathbf{u}}^{r_s} = (\tilde{u}_{00}^{r_s} \quad \cdots \quad \tilde{u}_{lm}^{r_s} \quad \cdots \quad \tilde{u}_{LL}^{r_s})^T, \quad (29)$$

the statement of our first problem is to solve

$$\arg \min_{\tilde{\mathbf{u}}^{r_s}} \|\mathbf{Y}^T \tilde{\mathbf{u}}^{r_s} - \mathbf{V}\|^2, \quad (30)$$

and the solution is given by

$$\tilde{\mathbf{u}}^{r_s} = (\mathbf{Y}\mathbf{Y}^T)^{-1} \mathbf{Y}\mathbf{V}. \quad (31)$$

3.2. P2: Scalar derivative data, scalar-harmonic potential coefficients, different altitudes

Let there be k values of the *radial component* of the derivative of the potential at satellite altitude r_s ,

$$\mathbf{V}'_r = \left(\nabla V(r_s \hat{\mathbf{r}}_1) \cdot \hat{\mathbf{r}} \quad \cdots \quad \nabla V(r_s \hat{\mathbf{r}}_k) \cdot \hat{\mathbf{r}} \right)^T, \quad \text{where} \quad \nabla V(r_s \hat{\mathbf{r}}) \cdot \hat{\mathbf{r}} = \sum_{l=0}^{\infty} \sum_{m=-l}^l A_{lm,lm} u_{lm}^{r_s} Y_{lm}(\hat{\mathbf{r}}). \quad (32)$$

We estimate the spherical-harmonic coefficients $u_{lm}^{r_e}$ of the potential on Earth's surface Ω_{r_e} , collectively

$$\tilde{\mathbf{u}}^{r_e} = (\tilde{u}_{00}^{r_e} \quad \cdots \quad \tilde{u}_{lm}^{r_e} \quad \cdots \quad \tilde{u}_{LL}^{r_e})^T. \quad (33)$$

which formulates our second problem as

$$\arg \min_{\tilde{\mathbf{u}}^{r_e}} \|\mathbf{Y}^T \mathbf{A} \tilde{\mathbf{u}}^{r_e} - \mathbf{V}'_r\|^2, \quad (34)$$

and its solution is found to be

$$\tilde{\mathbf{u}}^{r_e} = \mathbf{A}^{-1} (\mathbf{Y}\mathbf{Y}^T)^{-1} \mathbf{Y}\mathbf{V}'_r. \quad (35)$$

3.3. P3: Vector data, vector-harmonic coefficients, same altitude

Let there be $3k$ discrete function values of the *gradient* of the potential at satellite altitude r_s ,

$$\mathbf{V}' = \left(\mathbf{V}'_r{}^T \quad \mathbf{V}'_\theta{}^T \quad \mathbf{V}'_\phi{}^T \right)^T, \quad \text{where} \quad \nabla V(r_s \hat{\mathbf{r}}_i) = \sum_{l=0}^{\infty} \sum_{m=-l}^l v_{lm}^{r_s} \mathbf{E}_{lm}(\hat{\mathbf{r}}_i), \quad (36)$$

using the notation generalizing eq. (32), and let us estimate the gradient-vector coefficients in the vector

$$\tilde{\mathbf{v}}^{r_s} = (\tilde{v}_{00}^{r_s} \quad \cdots \quad \tilde{v}_{lm}^{r_s} \quad \cdots \quad \tilde{v}_{LL}^{r_s})^T, \quad (37)$$

in the basis of the gradient-vector spherical harmonics \mathbf{E}_{lm} . We also define the matrix of point-evaluations of the gradient-vector spherical harmonics

$$\mathbf{E} = (\mathbf{E}_r \quad \mathbf{E}_\theta \quad \mathbf{E}_\phi), \quad (38)$$

where the constituent matrices are given by

$$\mathbf{E}_r = \begin{pmatrix} \mathbf{E}_{00}(\hat{\mathbf{r}}_1) \cdot \hat{\mathbf{r}} & \cdots & \mathbf{E}_{00}(\hat{\mathbf{r}}_k) \cdot \hat{\mathbf{r}} \\ \vdots & & \vdots \\ \mathbf{E}_{LL}(\hat{\mathbf{r}}_1) \cdot \hat{\mathbf{r}} & \cdots & \mathbf{E}_{LL}(\hat{\mathbf{r}}_k) \cdot \hat{\mathbf{r}} \end{pmatrix}, \quad (39)$$

and similarly, *mutatis mutandis*, for the tangential components. Our third problem is thus to solve

$$\arg \min_{\tilde{\mathbf{v}}^{r_s}} \|\mathbf{E}^T \tilde{\mathbf{v}}^{r_s} - \mathbf{V}'\|^2, \quad (40)$$

which is equivalent to writing

$$\tilde{\mathbf{v}}^{r_s} = (\mathbf{E}\mathbf{E}^T)^{-1} \mathbf{E}\mathbf{V}'. \quad (41)$$

3.4. P4: Vector data, scalar-harmonic potential coefficients, different altitudes

Finally, we estimate the spherical-harmonic coefficients $u_{lm}^{r_e}$ of the potential on Earth's surface Ω_{r_e} , from gradient data collected at satellite altitude on Ω_{r_s} , in other words, we find

$$\arg \min_{\tilde{\mathbf{u}}^{r_e}} \|\mathbf{E}^T \mathbf{B} \tilde{\mathbf{u}}^{r_e} - \mathbf{V}'\|^2, \quad (42)$$

which has the solution

$$\tilde{\mathbf{u}}^{r_e} = \mathbf{B}^{-1}(\mathbf{E}\mathbf{E}^T)^{-1}\mathbf{E}\mathbf{V}'. \quad (43)$$

For every one of the solutions listed thus far in eqs (31), (35), (41), and (43), we require at least as many unique, non-nodal data points as there are coefficients to estimate, $k \geq (L+1)^2$, or $3k \geq (L+1)^2$ for the vectorial case, otherwise the matrices $(\mathbf{Y}\mathbf{Y}^T)$ and $(\mathbf{E}\mathbf{E}^T)$ will not be invertible. If we have data distributed only over a certain concentration region R , the matrices $(\mathbf{Y}\mathbf{Y}^T)$ or $(\mathbf{E}\mathbf{E}^T)$ will require regularization.⁹ Elsewhere³ we discuss the bias that arises from making bandlimited estimates (eqs 29, 33 and 37) from intrinsically wideband field observations (27) and (36), but in the remainder of this paper we will restrict our attention to purely bandlimited problems.

4. BASIS TRANSFORMATIONS FOR APPROXIMATION (AND INVERSION)

In the previous sections we showed how scalar, vectorial, and gradient-vector Slepian bases can be constructed (by optimization, solving spectral eigenvalue problems) from the canonical (vector) spherical harmonics, and we introduced a number of estimation problems in satellite geophysics. In this section we introduce some more notation, and the basis transformations that allow for sparse local *approximations* of spherical signals (without noise). In the remaining sections we then use these to transform *inverse* problems (with noise) that suffer from instability in the spherical-harmonic bases because of the localized nature of data collection, into problems that use as a basis the Slepian functions, pre-made and specifically localized to the area of interest or data availability. Stably forming *truncated* expansions rather than *damping* ill-posed ones leads to superior numerical performance and ease-of-use, with a clear understanding of the statistics of the solutions to boot.

4.1. Transformation to the scalar Slepian basis

Using the scalar Slepian basis defined in Section 1.2, writing G_α for the α th best-concentrated solution of eqs (5)–(6), we can write the representation of a *bandlimited* potential function $V(\hat{\mathbf{r}})$ in the equivalent forms

$$V(\hat{\mathbf{r}}) = \sum_{l=0}^L \sum_{m=-l}^l u_{lm} Y_{lm}(\hat{\mathbf{r}}) = \sum_{\alpha=1}^{(L+1)^2} s_\alpha G_\alpha(\hat{\mathbf{r}}). \quad (44)$$

An $(L+1)^2 \times J$ -dimensional matrix \mathbf{G}_J contains the sets \mathbf{g}_α , $\alpha = 1 \rightarrow J$, of $(L+1)^2$ harmonic coefficients of the J best-concentrated scalar Slepian functions, and its $(L+1)^2 \times [(L+1)^2 - J]$ -dimensional complement is $\mathbf{G}_{>J}$,

$$\mathbf{G}_J = (\mathbf{g}_1 \quad \cdots \quad \mathbf{g}_J), \quad \mathbf{G}_{>J} = (\mathbf{g}_{J+1} \quad \cdots \quad \mathbf{g}_{(L+1)^2}). \quad (45)$$

Similarly, a J -dimensional vector \mathcal{G}_J has the best-concentrated functions G_α , $\alpha = 1 \rightarrow J$, complemented by $\mathcal{G}_{>J}$,

$$\mathcal{G}_J = (G_1 \quad \cdots \quad G_J)^T, \quad \mathcal{G}_{>J} = (G_{J+1} \quad \cdots \quad G_{(L+1)^2})^T. \quad (46)$$

Denoting the $J \times J$ -dimensional diagonal matrix containing the J largest concentration ratios by $\mathbf{\Lambda}_J$, the orthogonality of the Slepian functions stipulates that

$$\mathbf{\Lambda}_J = \text{diag}(\lambda_1, \dots, \lambda_J) = \int_R \mathcal{G}_J \mathcal{G}_J^T d\Omega. \quad (47)$$

The Slepian functions allow for a constructive approximation of bandlimited functions of the kind $V(\hat{\mathbf{r}})$, locally within the target region R , by restricting the expansion (44) to the J best-concentrated Slepian functions,^{10,11}

$$V(\hat{\mathbf{r}}) \approx \sum_{\alpha=1}^J s_\alpha G_\alpha(\hat{\mathbf{r}}), \quad \hat{\mathbf{r}} \in R. \quad (48)$$

The greater the number of terms J , the less well localized the approximation, but the smaller the error.

4.2. Transformation to the gradient-vector Slepian basis

We transform a bandlimited gradient-vector function into its equivalent gradient-vector Slepian expansion

$$\nabla V(\hat{\mathbf{r}}) = \sum_{l=0}^L \sum_{m=-l}^l v_{lm} \mathbf{E}_{lm}(\hat{\mathbf{r}}) = \sum_{\alpha=1}^{(L+1)^2} t_{\alpha} \mathbf{H}_{\alpha}(\hat{\mathbf{r}}). \quad (49)$$

We introduce the $(L+1)^2 \times J$ dimensional matrix containing the $(L+1)^2$ -dimensional gradient-vector spherical-harmonic coefficient sets \mathbf{h}_{α} , $\alpha = 1 \rightarrow J$, for each of the J best-concentrated gradient-vector Slepian functions

$$\mathbf{H}_J = (\mathbf{h}_1 \quad \cdots \quad \mathbf{h}_J), \quad (50)$$

the J -dimensional vector containing the J best-concentrated gradient-vector Slepian functions

$$\boldsymbol{\mathcal{H}}_J = (\mathbf{H}_1 \quad \cdots \quad \mathbf{H}_J)^T, \quad (51)$$

and the $J \times J$ dimensional diagonal matrix containing the J largest concentration ratios, from orthogonality,

$$\boldsymbol{\Sigma}_J = \text{diag}(\sigma_1, \dots, \sigma_J) = \int_R \boldsymbol{\mathcal{H}}_J \cdot \boldsymbol{\mathcal{H}}_J^T d\Omega. \quad (52)$$

A local approximation of the gradient function can be obtained from

$$\nabla V(\hat{\mathbf{r}}) \approx \sum_{\alpha=1}^J t_{\alpha} \mathbf{H}_{\alpha}(\hat{\mathbf{r}}), \quad \hat{\mathbf{r}} \in R. \quad (53)$$

5. POTENTIAL FIELDS FROM RADIAL DATA USING SLEPIAN FUNCTIONS

With the scalar Slepian functions defined in Section 1.2 we now reformulate the solution to problem **P2** as a localized bandlimited potential-field estimation problem, from *noisy* radial-derivative data at satellite altitude. We use the Slepian functions to localize the radial-field analysis at satellite altitude and then downward-transform the resulting spherical-harmonic coefficients.

5.1. Discrete Formulation and Truncated Solutions

From pointwise data values of the radial derivative of the potential at satellite altitude, given at the points $r_s \hat{\mathbf{r}}_1, \dots, r_s \hat{\mathbf{r}}_k$, and polluted by noise,

$$\mathbf{d}_r = \mathbf{V}'_r + \mathbf{n}_r, \quad (54)$$

we seek to estimate the bandlimited partial set of corresponding spherical-harmonic coefficients of the scalar potential V on Earth's surface Ω_{r_e} , as in the original statement (34) of Problem **P2**. In eq. (54), \mathbf{V}'_r is defined as in eq. (32), and \mathbf{n}_r is a vector of noise values at the evaluation points.

As seen in eq. (35), the solution to problem **P2** involves the inversion of a “normal” matrix, $(\mathbf{Y}\mathbf{Y}^T)^{-1}$, that has many near-zero eigenvalues, and the additional accounting for the effects of altitude via the term \mathbf{A}^{-1} , which will potentially unstably inflate the smallest-scale noise terms.¹² Instead of regularization by *damping* (in the spherical-harmonic basis), the approach we propose is based on *truncation* (in the Slepian basis). We focus on the estimation of the radial field at satellite altitude in a chosen target region R , by estimating only its J best-concentrated Slepian coefficients. The hard truncation level J is a regularization parameter whose value needs to be chosen based on signal-to-noise considerations and an optimality criterion, much as a proper damping parameter would.^{9,13,14}

We codify our regularization of only solving for the coefficients of the J best-concentrated Slepian functions at satellite altitude by defining the $J \times k$ dimensional matrix containing the point evaluations of the J best-concentrated Slepian functions on the unit sphere,

$$\mathbf{G}_J = \mathbf{G}_J^T \mathbf{Y}, \quad (55)$$

and by solving, instead of eq. (34),

$$\arg \min_{\tilde{\mathbf{s}}_J^{r_s}} \|\mathbf{G}_J^T \tilde{\mathbf{s}}_J^{r_s} - \mathbf{d}_r\|^2, \quad (56)$$

for the J -dimensional vector $\tilde{\mathbf{s}}_J^{r_s}$ containing the coefficients of the approximation at satellite altitude in the bandlimited Slepian basis. When $J \leq k$ we have the solution

$$\tilde{\mathbf{s}}_J^{r_s} = (\mathbf{G}_J \mathbf{G}_J^T)^{-1} \mathbf{G}_J \mathbf{d}_r, \quad (57)$$

which we then downward-transform to the $(L+1)^2$ spherical-harmonic coefficients $\tilde{\mathbf{u}}^{r_e}$ of the field on Earth's surface Ω_{r_e} as

$$\tilde{\mathbf{u}}^{r_e} = \mathbf{A}^{-1} \mathbf{G}_J \tilde{\mathbf{s}}_J^{r_s} = \mathbf{A}^{-1} \mathbf{G}_J (\mathbf{G}_J \mathbf{G}_J^T)^{-1} \mathbf{G}_J \mathbf{d}_r. \quad (58)$$

The numerical conditioning of the matrix $(\mathbf{G}_J \mathbf{G}_J^T)$ is determined by the truncation parameter J , and we require the inverse of the matrix \mathbf{A} defined in eq. (22).

The resulting approximation $\tilde{V}(r_e \hat{\mathbf{r}})$ of the potential field $V(r_e \hat{\mathbf{r}})$ (at any point on Ω_{r_e}) can be calculated as

$$\tilde{V}(r_e \hat{\mathbf{r}}) = \mathcal{Y}^T \tilde{\mathbf{u}}^{r_e} = \mathcal{G}_{\downarrow J}^T (\mathbf{G}_J \mathbf{G}_J^T)^{-1} \mathbf{G}_J \mathbf{d}_r = \mathcal{G}_{\downarrow J}^T \tilde{\mathbf{s}}_J^{r_s}, \quad (59)$$

where we used $\mathcal{Y} = (Y_{00} \cdots Y_{LL})^T$ to collect the spherical harmonics for the bandwidth L , and defined the vector of the J best-concentrated downward-transformed scalar Slepian functions (and its complement) as

$$\mathcal{G}_{\downarrow J} = \mathbf{G}_J^T \mathbf{A}^{-1} \mathcal{Y}, \quad \mathcal{G}_{\downarrow > J} = \mathbf{G}_{> J}^T \mathbf{A}^{-1} \mathcal{Y}. \quad (60)$$

5.2. Continuous formulation and statistical considerations

The analytical counterpart to eq. (54) for data known (or desired) only within the target region R is

$$d(\hat{\mathbf{r}}) = \begin{cases} \partial_r V(r_s \hat{\mathbf{r}}) + n(\hat{\mathbf{r}}) & \text{if } \hat{\mathbf{r}} \in R \\ \text{unknown} & \text{if } \hat{\mathbf{r}} \in \Omega \setminus R, \end{cases} \quad (61)$$

where $n(\hat{\mathbf{r}})$ is the spatial noise function at satellite altitude r_s . The estimation problem equivalent to eq. (56), regularized by finding only the J best-concentrated Slepian coefficients that describe the data in eq. (61), is

$$\arg \min_{\tilde{\mathbf{s}}_J^{r_s}} \int_R (\mathcal{G}_J^T \tilde{\mathbf{s}}_J^{r_s} - d)^2 d\Omega. \quad (62)$$

Differentiating with respect to $\tilde{\mathbf{s}}_J^{r_s}$ to find the stationary points, and making use of eq. (47), the solution is

$$\tilde{\mathbf{s}}_J^{r_s} = \left(\int_R \mathcal{G}_J \mathcal{G}_J^T d\Omega \right)^{-1} \int_R \mathcal{G}_J d d\Omega = \mathbf{\Lambda}_J^{-1} \int_R \mathcal{G}_J d d\Omega. \quad (63)$$

As with the estimation of the spherical-harmonic coefficients of the potential field from the Slepian coefficients at altitude obtained from pointwise data in eq. (58) we can evaluate the field (anywhere on Earth's surface, although of course we target good recovery only in the region of interest) as

$$\tilde{V}(r_e \hat{\mathbf{r}}) = \mathcal{Y}^T \tilde{\mathbf{u}}^{r_e} = \mathcal{Y}^T \mathbf{A}^{-1} \mathbf{G}_J \mathbf{\Lambda}_J^{-1} \int_R \mathcal{G}_J d d\Omega = \mathcal{G}_{\downarrow J}^T \mathbf{\Lambda}_J^{-1} \int_R \mathcal{G}_J d d\Omega, \quad (64)$$

where the truncated vector of downward-transformed Slepian functions $\mathcal{G}_{\downarrow J}$ is defined in eq. (60).

The complete assessment of the statistical performance of the estimator (64) is difficult.^{13, 15–20} However, special cases are easy to come by and learn from.⁹ We make the following four oversimplified assumptions by which to obtain simple expressions for variance, bias, and, ultimately, mean squared error $\langle \epsilon^2 \rangle$:

1. The signal $V(r_e \hat{\mathbf{r}})$ is bandlimited, as are the Slepian functions $\mathcal{G}(\hat{\mathbf{r}})$, with the same bandwidth L .
2. The signal is — almost, given the incompatible stipulation 1 — “white” on Earth's surface, with power S .
3. The noise is white at the observation level, with power N .
4. The noise has zero mean and is uncorrelated with the signal.

As shown by us elsewhere,³ the mean squared estimation error in that case is given by

$$\langle \epsilon^2 \rangle = N \mathcal{G}_{\downarrow J}^T \mathbf{\Lambda}_J^{-1} \mathcal{G}_{\downarrow J} + S \mathcal{G}_{\downarrow > J}^T (\mathbf{G}_{> J}^T \mathbf{A}^2 \mathbf{G}_{> J}) \mathcal{G}_{\downarrow > J}. \quad (65)$$

6. POTENTIAL FIELDS FROM VECTORIAL DATA USING SLEPIAN FUNCTIONS

We now present a method to solve problem **P4**, the estimation of the potential field on Earth's or another planet's surface from noisy (three-component) vectorial data at satellite altitude.²¹ We will use the gradient-vector Slepian functions introduced in Section 4.2 to fit the local data at satellite altitude and then downward-transform the gradient-vector spherical-harmonic coefficients thus obtained.

6.1. Discrete Formulation and Truncated Solutions

Given pointwise data values of the gradient of the potential that are polluted by noise at the points $r_s \hat{\mathbf{r}}_1, \dots, r_s \hat{\mathbf{r}}_k$,

$$\mathbf{d} = \mathbf{V}' + \mathbf{n}, \quad (66)$$

where \mathbf{V}' is defined in eq. (36), and \mathbf{n} is a vector of noise values at the evaluation points for the individual components, we seek to estimate the spherical-harmonic coefficients of the scalar potential V on Earth's surface Ω_{r_e} , as in the statement (42) of problem **P4**. The solution eq. (43) contains the matrix inverse $(\mathbf{E}\mathbf{E}^T)^{-1}$ which again is intrinsically poorly conditioned. To regularize the problem we transform the problem into the gradient-vector Slepian basis for the relevant bandwidth L and the chosen target region R , and focus on estimating only the J best-concentrated gradient-vector Slepian coefficients. We leave the choice of the value J for later. As for the scalar case we apply regularization by only estimating the coefficients for the J best-concentrated gradient-vector Slepian functions. We define the $J \times 3k$ dimensional matrix containing the point evaluations of those,

$$\mathbf{H}_J = \mathbf{H}_J^T \mathbf{E}, \quad (67)$$

and then solve, instead of eq. (42),

$$\arg \min_{\tilde{\mathbf{t}}_J^{r_s}} \|\mathbf{H}_J^T \tilde{\mathbf{t}}_J^{r_s} - \mathbf{d}\|^2 \quad (68)$$

for the J -dimensional vector $\tilde{\mathbf{t}}_J^{r_s}$ of gradient-vector Slepian coefficients at satellite altitude. For $J \leq 3k$,

$$\tilde{\mathbf{t}}_J^{r_s} = (\mathbf{H}_J \mathbf{H}_J^T)^{-1} \mathbf{H}_J \mathbf{d} \quad (69)$$

is subsequently downward-transformed to the $(L+1)^2$ spherical-harmonic coefficients $\tilde{\mathbf{u}}^{r_e}$ of the field on Earth's surface Ω_{r_e} as

$$\tilde{\mathbf{u}}^{r_e} = \mathbf{B}^{-1} \mathbf{H}_J \tilde{\mathbf{t}}_J^{r_s} = \mathbf{B}^{-1} \mathbf{H}_J (\mathbf{H}_J \mathbf{H}_J^T)^{-1} \mathbf{H}_J \mathbf{d}, \quad (70)$$

using the matrix \mathbf{B} defined in eq. (24). The conditioning of the matrix $(\mathbf{H}_J \mathbf{H}_J^T)$ is determined by the truncation level J . The local approximation $\tilde{V}(r_e \hat{\mathbf{r}})$ of the potential field $V(r_e \hat{\mathbf{r}})$ can now be calculated by

$$\tilde{V}(r_e \hat{\mathbf{r}}) = \mathcal{Y}^T \tilde{\mathbf{u}}^{r_e} = \mathcal{H}_{\downarrow J}^T (\mathbf{H}_J \mathbf{H}_J^T)^{-1} \mathbf{H}_J \mathbf{d} = \mathcal{H}_{\downarrow J}^T \tilde{\mathbf{t}}_J^{r_s}, \quad (71)$$

where we have defined the vector of the J best-concentrated gradient-vector Slepian functions (and its complement) that are downward-transformed (hence, expanded in *scalar* spherical harmonics) as

$$\mathcal{H}_{\downarrow J} = \mathbf{H}_J^T \mathbf{B}^{-1} \mathcal{Y}, \quad \mathcal{H}_{\downarrow > J} = \mathbf{H}_{> J}^T \mathbf{B}^{-1} \mathcal{Y}. \quad (72)$$

Fig. 3 shows an example of the downward-transformed gradient-vector Slepian functions for North America.

6.2. Continuous formulation and statistical considerations

The data that are the functional equivalent of the point values (66) in the target region R are expressed as

$$\mathbf{d}(\hat{\mathbf{r}}) = \begin{cases} \nabla V(r_s \hat{\mathbf{r}}) + \mathbf{n}(\hat{\mathbf{r}}) & \text{if } \hat{\mathbf{r}} \in R \\ \text{unknown} & \text{if } \hat{\mathbf{r}} \in \Omega \setminus R, \end{cases} \quad (73)$$

where $\mathbf{n}(\hat{\mathbf{r}})$ is a vector valued function of space describing the noise at satellite altitude r_s . The problem equivalent to eq. (68), regularized by solving only for the coefficients of the J best-concentrated gradient-vector Slepian functions at altitude, to fit the data \mathbf{d} given in eq. (73), is

$$\arg \min_{\tilde{\mathbf{t}}_J^{r_s}} \int_R \left(\mathcal{H}_J^T \tilde{\mathbf{t}}_J^{r_s} - \mathbf{d} \right)^2 d\Omega = \arg \min_{\tilde{\mathbf{t}}_J^{r_s}} \int_R \left(\mathcal{H}_J^T \tilde{\mathbf{t}}_J^{r_s} - \mathbf{d} \right) \cdot \left(\mathcal{H}_J^T \tilde{\mathbf{t}}_J^{r_s} - \mathbf{d} \right) d\Omega, \quad (74)$$

which is solved by

$$\tilde{t}_J^{r_s} = \left(\int_R \mathcal{H}_J \cdot \mathcal{H}_J^T d\Omega \right)^{-1} \int_R \mathcal{H}_J \cdot \mathbf{d} d\Omega = \Sigma_J^{-1} \int_R \mathcal{H}_J \cdot \mathbf{d} d\Omega, \quad (75)$$

where we have used eq. (52). As for the pointwise data case shown in eq. (70) we can transform the coefficients $\tilde{\mathbf{u}}^{r_e}$ obtained from the data \mathbf{d} by eq. (71) into a local estimate of the potential field at the Earth's surface as

$$\tilde{V}(r_e \hat{\mathbf{r}}) = \mathcal{Y}^T \tilde{\mathbf{u}}^{r_e} = \mathcal{Y}^T \mathbf{B}^{-1} \mathbf{H}_J \Sigma_J^{-1} \int_R \mathcal{H}_J \cdot \mathbf{d} d\Omega = \mathcal{H}_{\downarrow J}^T \Sigma^{-1} \int_R \mathcal{H}_J \cdot \mathbf{d} d\Omega, \quad (76)$$

where the vector containing the downward-transformed gradient-vector Slepian functions $\mathcal{H}_{\downarrow J}$ is in eq. (72).

Even more so than for the scalar case described in Section 5.2, the calculation of the variance, bias, and mean squared error of the estimate (76) would be very involved without imparting much insight. Instead, as for the scalar case, we narrow our scope to vectorial data \mathbf{d} that involve white signals, white, zero-mean and uncorrelated vectorial noise.³ In that case, the mean squared estimation error is

$$\langle \epsilon^2 \rangle = N \mathcal{H}_{\downarrow J}^T \Sigma_J^{-1} \mathcal{H}_{\downarrow J} + S \mathcal{H}_{\downarrow > J}^T (\mathbf{H}_{> J}^T \mathbf{B}^2 \mathbf{H}_{> J}) \mathcal{H}_{\downarrow > J}. \quad (77)$$

7. NUMERICAL EXAMPLES: THE CASE OF NORTH AMERICA

In this section we illustrate eqs (58)–(59) to solve the noisy scalar problem **P2**, and eqs (70)–(71) for the noisy vectorial problem **P4**. In both cases we estimate a scalar potential field on Earth's surface from noisy scalar and vectorial data, synthesized at $(r_s - r_e) = 500$ km above Earth's surface. The “true” potential field $V(r_e \hat{\mathbf{r}}) = \mathcal{Y}^T \mathbf{u}^{r_e}$ is zero-mean, isotropic, with constant power contained within a bandwidth $L = 72$. Figs 4 and 6 show the potential-field signal in their upper-left panels. In all experiments we sampled the fields at altitude at the same set of 2951 points uniformly distributed over the target region R , North America, of solid-angle area $a = \int_R d\Omega$. From these points we created vectors with the data \mathbf{d}_r or \mathbf{d} as in eqs (54) and (66), the noise being Gaussian with a variance of 2.5% of the numerical signal power at r_s in each of the components.

At each fixed Slepian-basis truncation level J , the scalar estimates in eq. (58) are derived from the solutions (57) which minimize the quadratic misfit (56) that is our regularized proxy for the noisy version of problem (34). Similarly, the vectorial estimates eq. (70) derive from the solutions (69) to the misfit (68) which is our regularized version of the noisy version of problem (42). The truncation regularization biases the estimates by an amount that grows when lowering J (more truncation), but the estimation variances are positively affected by lowering J (which leads to smaller variance). We evaluate the quality of the estimates made using different truncation levels J in terms of their mean squared errors, whose behavior we understand from eqs (65) and (77).

For each experiment, as a measure of efficiency, we will compute the mean squared error between the estimated potential-field and the (bandlimited) truth, at the Earth's surface, averaged over the area of interest, as follows

$$\text{mse} = \frac{1}{a} \int_R [V(r_e \hat{\mathbf{r}}) - \tilde{V}(r_e \hat{\mathbf{r}})]^2 d\Omega. \quad (78)$$

We will express the regional mean squared error relative to the mean squared signal strength over the same area,

$$\text{mss} = \frac{1}{a} \int_R V^2(r_e \hat{\mathbf{r}}) d\Omega. \quad (79)$$

We will call the relative measure

$$\varphi(J) = \text{mse}/\text{mss}, \quad (80)$$

and plot it in function of the Slepian-function truncation level J . Finally, we will also quote the relative quadratic measure of data misfit, eq. (56), between the given data \mathbf{d}_r and the simulated data, $\mathbf{Y}^T \mathbf{A} \tilde{\mathbf{u}}^{r_e}$,

$$\psi(J) = \|\mathbf{Y}^T \mathbf{A} \tilde{\mathbf{u}}^{r_e} - \mathbf{d}_r\|^2 / \|\mathbf{d}_r\|^2, \quad (81)$$

where we recall that the prediction $\tilde{\mathbf{u}}^{r_e}$ is given by eq. (58) and thereby remains a function of the truncation level J . In the vectorial case, the metric is the relative mean squared data misfit, eq. (68), between the three vectorial components of the given data \mathbf{d} and the three vectorial components of the simulated data $\mathbf{E}^T \mathbf{B} \tilde{\mathbf{u}}^{r_e}$,

$$\psi(J) = \|\mathbf{E}^T \mathbf{B} \tilde{\mathbf{u}}^{r_e} - \mathbf{d}\|^2 / \|\mathbf{d}\|^2. \quad (82)$$

7.1. Potential field at the surface from radial-component data at satellite altitude

Fig. 4 shows the results from an experiment with noisy radial-derivative data. We used the same color map, scaled to the maximum absolute value of the truth $V(r_e \hat{\mathbf{r}})$ (points with absolute value smaller than 1% of the maximum are left white), except for the data, \mathbf{d}_r , one realization of which is shown in the top right, and whose values at r_s are attenuated compared to at r_e . The best estimate, $\tilde{V}(r_e \hat{\mathbf{r}})$, is plotted at Earth's surface Ω_{r_e} , calculated from eq. (59), with the Slepian-function truncation level $J = 346$. The error of eq. (81) is 0.1236. For this J the estimate approximates the truth very well within North America, with little energy outside.

Fig. 5 (left) shows 64 gray curves of $\varphi(J)$, the relative *model* error of eq. (80). The same true V_r' were used to make the data \mathbf{d}_r with different realization of the noise field \mathbf{n}_r . Overall, less truncation (larger J) reduces the estimation bias but increases the variance. The model errors φ do not improve immediately, unlike the *data* misfits $\psi(J)$, which decrease fast to the relative noise energy, 2.5%. There is a local minimum, followed by a rise, and then a decisive decline. We recall that we are minimizing the misfit of the upward-transformed potential field at the altitude of the data (see eq. 62) instead of the misfit on the surface, which is measured by φ . These details are well explained by the competition of terms in the theoretical relation (65), which, includes the effects of the potentially poorly-conditioned downward-transformation of the radial-field estimate at altitude truncation.

7.2. Potential field at the surface from gradient-vector data at satellite altitude

Fig. 6 shows the results from an experiment with noisy vectorial data conducted in the same vein. We used eq. (71) to calculate an estimate $\tilde{V}(r_e \hat{\mathbf{r}})$ for the potential field on Earth's surface, again choosing the Slepian truncation $J = 421$ based on the numerical experimentation. The best-estimated field $\tilde{V}(r_e \hat{\mathbf{r}})$ approximates the true signal $V(r_e \hat{\mathbf{r}})$ well within North America with the relative model error of eq. (80) being 0.0479.

In Fig. 5 (right) we plot the model errors $\varphi(J)$ of eq. (80) as a function of the truncation level J , for each of the 64 experiments. Again, each data set \mathbf{d} is generated from the same true vector field V' using eq. (66), but differs by the realization of the noise \mathbf{n} . The theoretical relation in eq. (77) explains how the decreasing bias and increasing variance trade off as a function of the increasing number J of Slepian functions. As in the scalar case the curves $\varphi(J)$ go through a local minimum before reaching the global optimum truncation level. Indeed, since we minimized eq. (74) at altitude, in order to obtain the estimate $\tilde{V}(r_e \hat{\mathbf{r}})$ at the Earth's surface we need to apply the downward-transformation operator \mathbf{B} defined in eq. (24). At high maximum degrees L and high relative satellite altitudes r_s/r_e this operator is poorly conditioned. The interaction between the various competing effects produces a complex but reproducible error behavior. As for the scalar case, the relative mean squared data misfit $\psi(J)$ decreases fast until it reaches the relative energy of the noise, 2.5%, indicated by the dashed horizontal black line.

8. CONCLUSIONS

As is the case for scalar functions (see ref. 1), we can construct a geographically concentrated orthogonal family of bandlimited *vector* spherical-harmonic fields on the unit sphere by solving algebraic eigenvalue problems. Vectorial "Slepian" functions on the sphere are a tool for the analysis and representation of space- and bandlimited spherical vector functions. In this contribution we reviewed their construction (from ref. 2) and introduced their use in the constructive approximation of vectorial signals on the sphere, with applications in satellite geophysics. For the specific situation where harmonic potential fields are being analyzed, we prefer using linear combinations of vector-spherical harmonics, termed *gradient-vector* harmonics, which can be downward- and upward continued from the Earth's surface to satellite with analytical simplicity (if not stability). From these building blocks we have also constructed Slepian functions (in ref. 3) that we review here. Finally, we reviewed the properties of two methods to estimate a potential field from localized gradient data at satellite altitude. The first method operates on radial-component data and uses a truncated basis of scalar Slepian functions. The second considers all three data components and uses gradient-vector Slepian functions. We illustrate how the reconstruction error depends on the number of Slepian functions used for the estimation. While this paper combines and (much!) condenses material published by ourselves elsewhere, all of the examples shown are new and original.

ACKNOWLEDGMENTS

Financial support has been provided by the U. S. National Science Foundation under EAR-1150145 to FJS.

REFERENCES

1. F. J. Simons, F. A. Dahlen, and M. A. Wieczorek, "Spatiospectral concentration on a sphere," *SIAM Rev.* **48**(3), pp. 504–536, doi: 10.1137/S0036144504445765, 2006.
2. A. Plattner and F. J. Simons, "Spatiospectral concentration of vector fields on a sphere," *Appl. Comput. Harmon. Anal.*, p. doi:10.1016/j.acha.2012.12.001, 2013.
3. A. Plattner and F. J. Simons, "Potential-field estimation using scalar and vector Slepian functions at satellite altitude," pp. submitted, available on [arXiv:1306.6550](https://arxiv.org/abs/1306.6550), 2014.
4. N. Olsen, G. Hulot, and T. J. Sabaka, "Sources of the geomagnetic field and the modern data that enable their investigation," in *Handbook of Geomathematics*, W. Freeden, M. Z. Nashed, and T. Sonar, eds., ch. 5, pp. 105–124, doi: 10.1007/978-3-642-01546-5_5, Springer, Heidelberg, Germany, 2010.
5. R. A. Langel and W. J. Hinze, *The Magnetic Field of the Earth's Lithosphere: The Satellite Perspective*, Cambridge Univ. Press, Cambridge, UK, 1998.
6. F. J. Lowes, A. de Santis, and B. Duka, "A discussion of the uniqueness of a Laplacian potential when given only partial field information on a sphere," *Geophys. J. Int.* **121**(2), pp. 579–584, 1995.
7. C. Mayer and T. Maier, "Separating inner and outer Earth's magnetic field from CHAMP satellite measurements by means of vector scaling functions and wavelets," *Geophys. J. Int.* **167**, pp. 1188–1203, doi: 10.1111/j.1365-246X.2006.03199.x, 2006.
8. W. Freeden and M. Schreiner, *Spherical Functions of Mathematical Geosciences: A Scalar, Vectorial, and Tensorial Setup*, Springer, Berlin, 2009.
9. F. J. Simons and F. A. Dahlen, "Spherical Slepian functions and the polar gap in geodesy," *Geophys. J. Int.* **166**, pp. 1039–1061, doi: 10.1111/j.1365-246X.2006.03065.x, 2006.
10. F. J. Simons, J. C. Hawthorne, and C. D. Beggan, "Efficient analysis and representation of geophysical processes using localized spherical basis functions," in *Wavelets XIII*, V. K. Goyal, M. Papadakis, and D. Van de Ville, eds., **7446**, pp. 74460G, doi: 10.1117/12.825730, SPIE, 2009.
11. C. D. Beggan, J. Saarimäki, K. A. Whaler, and F. J. Simons, "Spectral and spatial decomposition of lithospheric magnetic field models using spherical Slepian functions," *Geophys. J. Int.* **193**(1), pp. 136–148, doi: 10.1093/gji/ggs122, 2013.
12. S. Maus, M. Rother, C. Stolle, W. Mai, S. Choi, H. Lühr, D. Cooke, and C. Roth, "Third generation of the Potsdam Magnetic Model of the Earth (POMME)," *Geochem. Geophys. Geosys.* **7**, pp. Q07008, doi: 10.1029/2006GC001269, 2006.
13. W. M. Kaula, "Theory of statistical analysis of data distributed over a sphere," *Rev. Geophys.* **5**(1), pp. 83–107, 1967.
14. M. A. Wieczorek and F. J. Simons, "Minimum-variance spectral analysis on the sphere," *J. Fourier Anal. Appl.* **13**(6), pp. 665–692, doi: 10.1007/s00041-006-6904-1, 2007.
15. K. A. Whaler and D. Gubbins, "Spherical harmonic analysis of the geomagnetic field: an example of a linear inverse problem," *Geophys. J. Int.* **65**(3), pp. 645–693, doi: 10.1111/j.1365-246X.1981.tb04877.x, 1981.
16. P. Xu, "The value of minimum norm estimation of geopotential fields," *Geophys. J. Int.* **111**, pp. 170–178, 1992.
17. P. Xu, "Truncated SVD methods for discrete linear ill-posed problems," *Geophys. J. Int.* **135**(2), pp. 505–514, doi: 10.1046/j.1365-246X.1998.00652.x, 1998.
18. R. Schachtschneider, M. Holschneider, and M. Mandea, "Error distribution in regional inversion of potential field data," *Geophys. J. Int.* **181**, pp. 1428–1440, doi: 10.1111/j.1365-246X.2010.04598.x, 2010.
19. R. Schachtschneider, M. Holschneider, and M. Mandea, "Error distribution in regional modelling of the geomagnetic field," *Geophys. J. Int.* **191**, pp. 1015–1024, doi: 10.1111/j.1365-246X.2012.05675.x, 2012.
20. D. C. Slobbe, F. J. Simons, and R. Klees, "The spherical Slepian basis as a means to obtain spectral consistency between mean sea level and the geoid," *J. Geodesy* **86**(8), pp. 609–628, doi: 10.1007/s00190-012-0543-x, 2012.
21. J. Arkani-Hamed, "An improved 50-degree spherical harmonic model of the magnetic field of Mars derived from both high-altitude and low-altitude data," *J. Geophys. Res.* **107**(E10), pp. 5083, doi: 10.1029/2001JE001835, 2002.

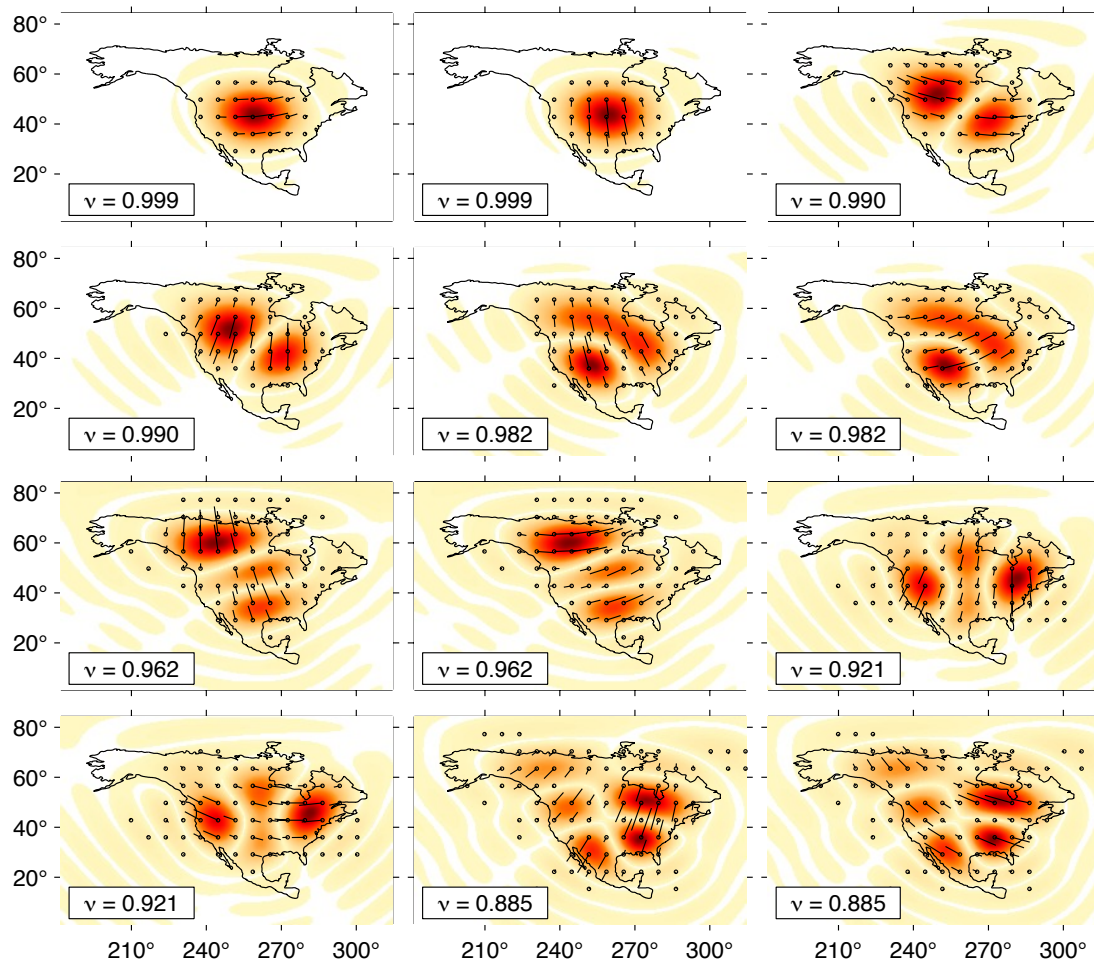


Figure 1. Twelve tangential Slepian functions $\mathbf{g}_1, \mathbf{g}_2, \dots, \mathbf{g}_{12}$, bandlimited to $L = 18$, optimally concentrated within North America. The concentration factors $\nu_1, \nu_2, \dots, \nu_{12}$ are indicated. The rounded tangential Shannon number $N^t = 29$. Order of concentration is left to right, top to bottom. Color is absolute value (red the maximum) and circles with strokes indicate the direction of the eigenfield on the tangential plane. Regions in which the absolute value is less than one hundredth of the maximum absolute value on the sphere are left white.

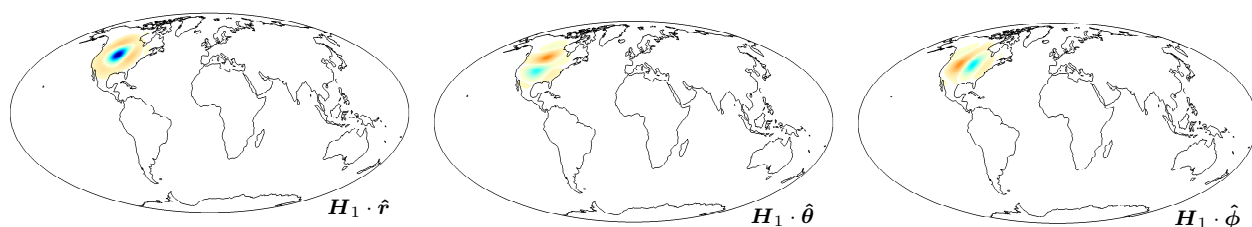


Figure 2. The three vectorial components of the gradient-vector Slepian function \mathbf{H}_1 , best concentrated to North America at a bandwidth $L = 30$. Left panel shows the radial component $\mathbf{H}_1 \cdot \hat{\mathbf{r}}$, center panel the colatitudinal component $\mathbf{H}_1 \cdot \hat{\boldsymbol{\theta}}$, and right panel the longitudinal component $\mathbf{H}_1 \cdot \hat{\boldsymbol{\phi}}$. The concentration coefficient, $\sigma = 0.999264$.

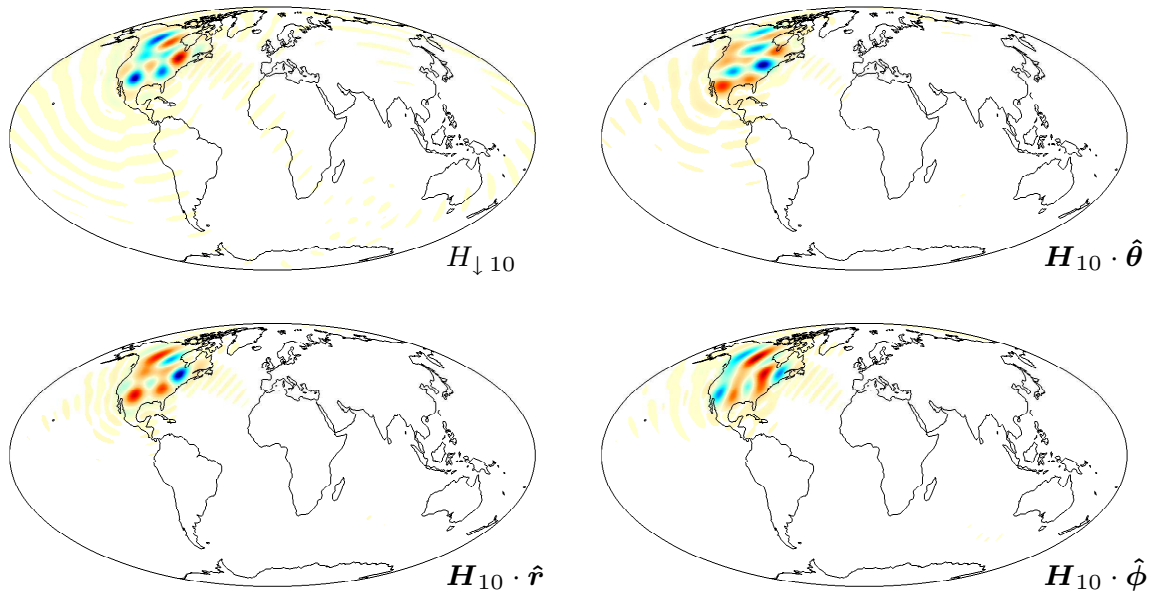


Figure 3. Downward transformation of the tenth best-concentrated gradient-vector Slepian function \mathbf{H}_{10} , at a spherical-harmonic bandwidth $L = 30$, for North America. The concentration coefficient $\sigma = 0.967882$ at altitude. Bottom and right panels show the radial and tangential components of the vector function \mathbf{H}_{10} . The top left panel shows the scalar potential $H_{\perp 10}$ that corresponds to the vector field \mathbf{H}_{10} at a distance 500 km below the “satellite altitude” of the latter.

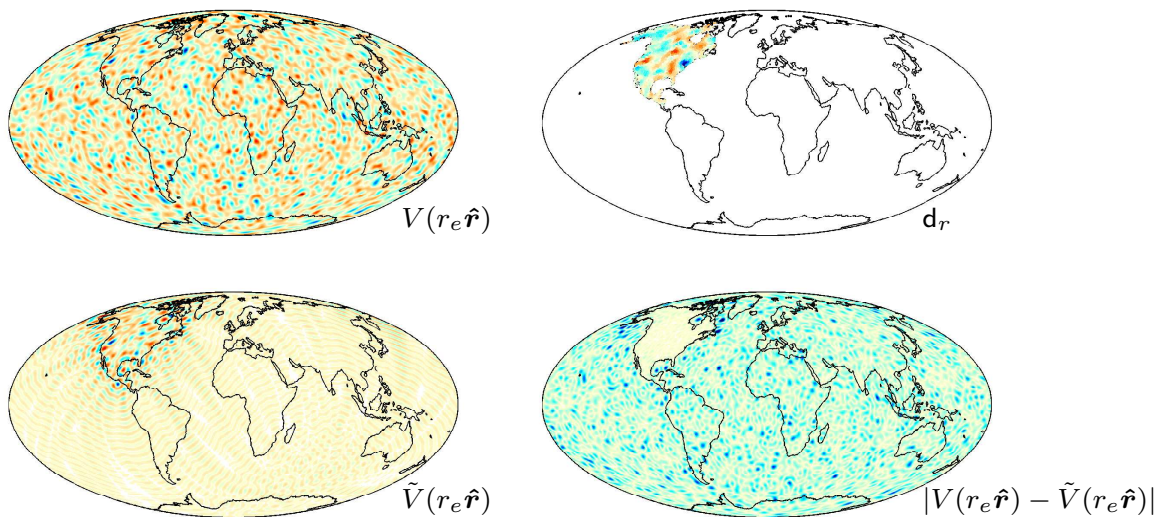


Figure 4. Example of the estimation of a potential field on Earth’s surface from noisy radial-derivative data at satellite altitude $r_s = r_e + 500$ km, using Slepian functions bandlimited to $L = 72$ and spatially concentrated to the target region North America. The upper left panel shows the true potential field $V(r_e \hat{\mathbf{r}})$ on Earth’s surface. The upper right panel shows the 2951 noisy data \mathbf{d}_r at satellite altitude. The middle left panel shows the estimated potential field $\tilde{V}(r_e \hat{\mathbf{r}})$ calculated from the data using eq. (59), with Slepian-function truncation level $J = 346$. The lower left panel shows the absolute value of the difference $|V(r_e \hat{\mathbf{r}}) - \tilde{V}(r_e \hat{\mathbf{r}})|$ between the true and the estimated potential fields.

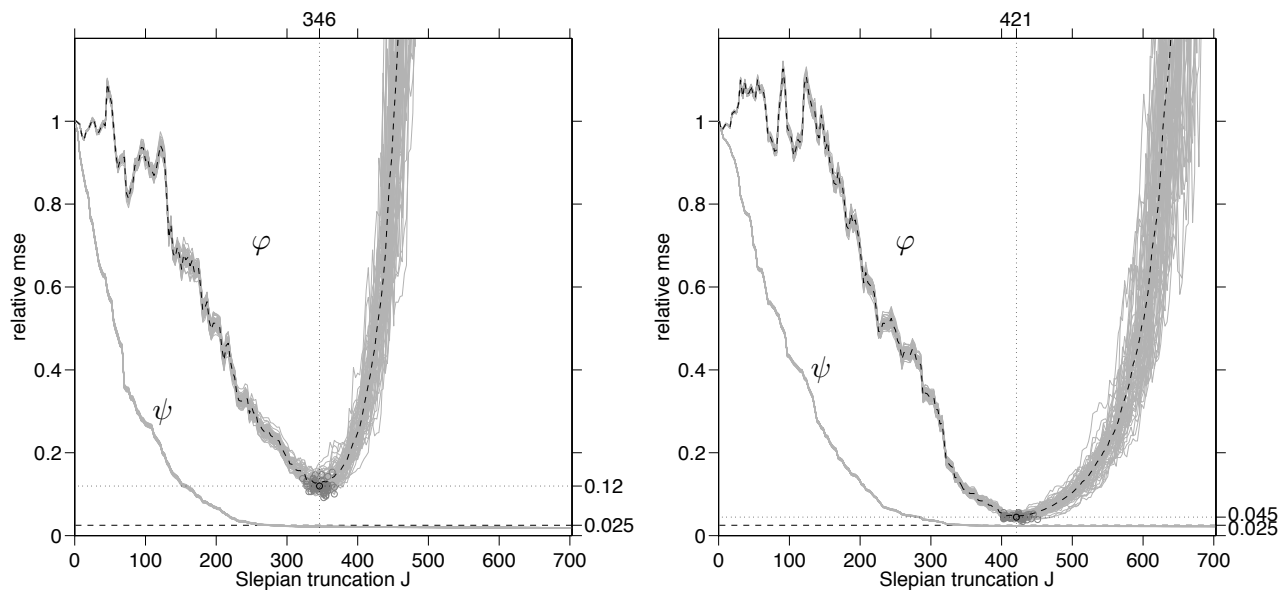


Figure 5. Relative regional mean squared model errors $\varphi(J)$, from eq. (80), and relative mean squared data misfit $\psi(J)$, from eq. (81), for potential field estimation from (left) radial-derivative data as described in eq. (59) and (right) vectorial data described in eq. (71). The true signals are shown in Figs 4. Each of the 64 noise realizations leads to a gray $\varphi(J)$ curve and a gray $\psi(J)$. Optimal truncation points are indicated by gray circles, average optimal truncation point by a black circle and average $\varphi(J)$ behavior is the black dashed line. The dashed horizontal line is the relative noise energy.

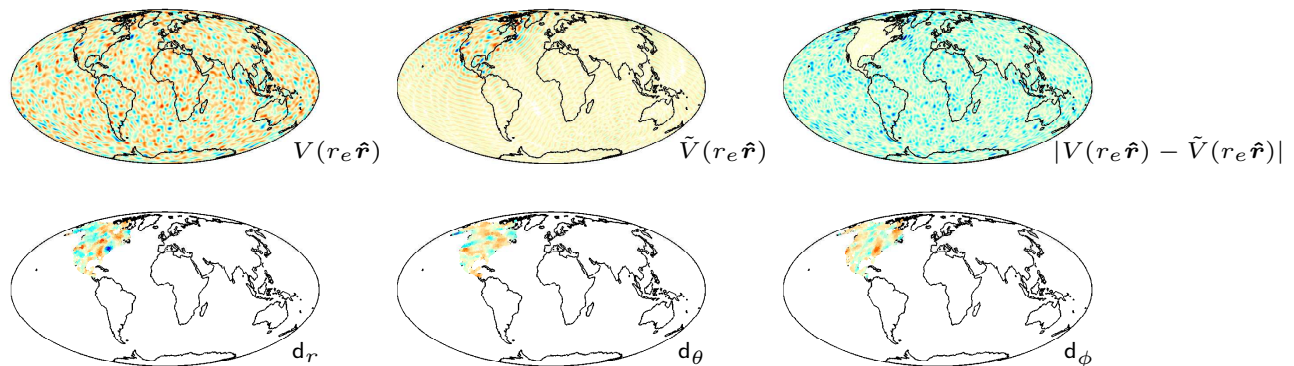


Figure 6. Example of a potential field estimation on Earth's surface from noisy gradient data at altitude $r_s = r_e + 500$ km for Slepian functions with maximum degree $L = 72$ and target region North America. The upper left panel shows the true potential field $V(r_e \hat{r})$ on Earth's surface. The three right panels show the noisy data \mathbf{d} at satellite altitude given by 2951 data values. The top right panel depicts the radial component d_r , the middle right panel the colatitudinal component d_θ , and the lower right panel the longitudinal component d_ϕ . The middle left panel shows the estimated potential field $\tilde{V}(r_e \hat{r})$ calculated from the data with Slepian truncation $J = 421$. The lower left panel shows the absolute difference $|V(r_e \hat{r}) - \tilde{V}(r_e \hat{r})|$ between the true and the estimated potential fields.